

# Computational Enhancement for Day-Ahead Energy Scheduling with Sparse Neural Network-based Battery Degradation Model

Cunzhi Zhao, *Student Member, IEEE* and Xingpeng Li, *Senior Member, IEEE*

**Abstract**— Battery energy storage systems (BESS) play a pivotal role in future power systems as they contribute to achieving the net-zero carbon emission objectives. The BESS systems, predominantly employing lithium-ion batteries, have been extensively deployed. The degradation of these batteries significantly affects system efficiency. Deep neural networks can accurately quantify the battery degradation, however, the model complexity hinders their applications in energy scheduling for various power systems at different scales. To address this issue, this paper presents a novel approach, introducing a linearized sparse neural network-based battery degradation model (SNNBD), specifically tailored to quantify battery degradation based on the scheduled BESS daily operational profiles. By leveraging sparse neural networks, this approach achieves accurate degradation prediction while substantially reducing the complexity associated with a dense neural network model. The computational burden of integrating battery degradation into day-ahead energy scheduling is thus substantially alleviated. Case studies, conducted on both microgrids and bulk power grids, demonstrated the efficiency and suitability of the proposed SNNBD-integrated scheduling model that can effectively address battery degradation concerns while optimizing day-ahead energy scheduling operations.

**Index Terms**— Battery degradation modeling, Bulk power grids, Day-ahead scheduling, Energy management, Machine learning, Microgrids, Optimization, Sparse neural network.

## NOMENCLATURE

### Indices:

$g$	Generator index.
$s$	Battery energy storage system index.
$k$	Transmission line index.
$l$	Load index.
$wt$	Wind turbine index.
$pv$	Photovoltaic index.

### Sets:

$T$	Set of time intervals.
$G$	Set of controllable micro generators.
$S$	Set of energy storage systems.
$WT$	Set of wind turbines.
$PV$	Set of PV systems.

### Parameters:

$c_g$	Linear cost for controllable unit $g$ .
$c_g^{NL}$	No load cost for controllable unit $g$ .
$c_g^{SU}$	Start-up cost for controllable unit $g$ .
$\Delta T$	Length of a single dispatch interval.
$R_{prcnt}$	Ratio of the backup power to the total power.
$E_s^{Max}$	Maximum energy capacity of ESS $s$ .

$E_s^{min}$	Minimum energy capacity of ESS $s$ .
$c_t^{Buy}$	Wholesale electricity purchase price in time interval $t$ .
$c_t^{Sell}$	Wholesale electricity sell price in time interval $t$ .
$p_g^{Max}$	Maximum capacity of generator $g$ .
$p_g^{Min}$	Minimum capacity of generator $g$ .
$p_k^{Max}$	Maximum thermal limit of transmission line $k$ .
$b_k$	Susceptance, inverse of impedance, of branch $k$ .
$p_{Grid}^{Max}$	Maximum thermal limit of tie-line between main grid and microgrid.
$p_g^{Ramp}$	Ramping limit of diesel generator $g$ .
$p_s^{Max}$	Maximum charge/discharge power of BESS $s$ .
$p_s^{Min}$	Minimum charge/discharge power of BESS $s$ .
$\eta_s^{Disc}$	Discharge efficiency of BESS $s$ .
$\eta_s^{Char}$	Charge efficiency of BESS $s$ .

### Variables:

$U_t^{Buy}$	Status of buying power from main grid in time interval $t$ .
$U_t^{Sell}$	Status of selling power to main grid status in time $t$ .
$U_{s,t}^{Char}$	Charging status of energy storage system $s$ in time interval $t$ . It is 1 if charging status; otherwise 0.
$U_{s,t}^{Disc}$	Discharging status of energy storage system $s$ in time interval $t$ . It is 1 if discharging status; otherwise 0.
$U_{g,t}$	Status of generator $g$ in time interval $t$ . It is 1 if on status; otherwise 0.
$V_{g,t}$	Startup indicator of Status of generator $g$ in time interval $t$ . It is 1 if unit $g$ starts up; otherwise 0.
$P_{g,t}$	Output of generator $g$ in time interval $t$ .
$\theta_{n(k)}^t$	Phase angle of sending bus $n$ of branch $k$ .
$\theta_{m(k)}^t$	Phase angle of receiving bus $m$ of branch $k$ .
$P_{k,t}$	Line flow at transmission line $k$ at time period $t$ .
$p_t^{Buy}$	Amount of power purchased from main grid power in time interval $t$ .
$p_t^{Sell}$	Amount of power sold to main grid power in time interval $t$ .
$P_{l,t}$	Demand of the microgrid in time interval $t$ .
$p_{s,t}^{Disc}$	Discharging power of energy storage system $s$ at time $t$ .
$p_{s,t}^{Char}$	Charging power of energy storage system $s$ at time $t$ .

## I. INTRODUCTION

Renewable energy sources (RES) have emerged as a pivotal component of the future power system, due to their environmental friendly attributes in contrast to conventional fossil fuels. By producing clean, sustainable, and inexhaustible electric energy, RES plays a transformative role in reducing greenhouse gas emissions in the electricity sector and thus mitigating climate change [1]. Nonetheless, the escalating utilization of RES for power generation has introduced inherent stability challenges in the system, primarily due to the unpredictable and intermittent nature of deeply integrated RES [2]–[4]. In response to this challenge, battery energy storage

systems (BESS) are being extensively adopted as an effective and practically viable solution [5].

BESS effectively addresses the variability and uncertainty inherent in RES by efficiently storing excess renewable energy during peak periods and releasing it during off-peak periods of renewable generation [6]. This capability not only promotes a seamless integration of renewable energy in the grid but also reinforces the resilience of the system. Furthermore, BESS plays a pivotal role in providing essential ancillary services such as frequency regulation, voltage control, and peak shaving, thereby enhancing the stability and efficiency of the overall power system [7]-[8].

Numerous studies have demonstrated the successful integration of BESS into both bulk power systems and microgrids, particularly those integrating high penetrations of RES. For instance, [9]-[10] demonstrate the microgrid's ability to support the main grid with integrated BESS. Moreover, [11] highlights the significant benefits of incorporating BESS into the power system. Another notable example is the offshore BESS system presented in [12], which effectively reduces carbon emissions. Various other models have been proposed to incorporate BESS to mitigate fluctuations caused by renewable energy sources, as presented in [13]-[16]. In summary, the deployment of BESS is indispensable for the successful integration of renewable energy into the power system. It not only improves the system's stability and efficiency but also paves the way for a cleaner and more sustainable energy future.

The primary component utilized in BESS presently available in the market is lithium-ion batteries [17]. However, these batteries' chemical characteristics make them susceptible to degrade over cycling, ultimately resulting in a negative impact on their performance and efficiency. The degradation of lithium-ion batteries is primarily attributed by the depletion of Lithium ions, electrolyte, and the escalation of internal resistance. Those changes contribute to an increase in internal resistance, and decrease the overall available energy capacity during daily cycling [19]-[20]. Multiple factors contribute to battery aging, including ambient temperature, charging/discharging rate, state of charge (SOC), state of health (SOH), and depth of discharge (DOD), each playing a pivotal role in the degradation process over the battery cycling [21]-[22]. Nevertheless, accurately assessing the internal state of the battery remains a difficult challenge. This complexity is particularly amplified by the escalating significance of batteries functioning as energy storage systems in both microgrid systems and bulk power systems. Thus, accurately quantifying battery degradation is an urging task, particularly when BESS operates in diverse conditions and environments in the power system.

Previous studies have extensively developed battery degradation models. However, these models fail to comprehensively address battery degradation across diverse operational conditions. One widely used approach is the DOD-based battery degradation model. Papers [23]-[27] proposed battery degradation models that depend on the DOD of each individual cycle. While this approach may be effective under consistent operating environments, it falls short when applied to the complex and diverse daily cycling scenarios of BESS. The DOD-based model omits various factors that can significantly contribute to substantial prediction errors in degradation. Another frequently employed model is the linear degradation

model. As discussed in [28], this model incorporates a linear degradation cost based on power usage or energy consumption within the battery degradation model. However, similar to the DOD-based model, it can only offer a rough estimation of battery degradation and is not suitable for accurate predictions in daily day-ahead scheduling problems due to its limited accuracy. Therefore, despite the existence of previous research on battery degradation models, none of these approaches adequately addresses the battery aging factors in BESS operations comprehensively.

In our previous research work [29], we applied a data-driven approach that utilized a neural network to accurately quantify battery degradation value. Distinct from the DOD-based and linear degradation models, our neural network-based battery degradation (NNBD) model takes into account various factors such as SOC, DOD, ambient temperature, charge or discharge rate, and SOH for each cycle, resulting in more precise degradation quantification. However, the highly non-linear and non-convex nature of the NNBD model poses challenges when seeking direct solutions to the day-ahead scheduling optimization problem. To address this challenge, we proposed a neural network and optimization decoupled heuristic algorithm in our previous work, which solves the complex neural network-embedded optimization problem iteratively. While the proposed iterative methodology exhibited commendable efficiency with the simple problems, unfortunately, its performance faltered when confronted with the complexities of a multi-BESS day-ahead scheduling optimization problem. The iteration method failed to converge when applied to a system with multiple integrated BESSs.

To overcome the non-linearity characteristic of the neural network-based day-ahead scheduling problem, we present a piecewise linear model in this paper. This model enables us to directly solve the optimization problem without relying on an iterative method mentioned in our previous work. The non-linearity within the NNBD model arises from the adoption of the rectified linear unit (ReLU) activation function in the hidden layer neurons. The linearized model, using the BigM method, is designed to linearize a ReLU activation function through the introduction of four linear constraints with an auxiliary binary variable. This allows for the direct solution of the NNBD-integrated day-ahead scheduling problem. However, when multiple BESSs are present in the system, a severe computational challenge would be observed. As the number of BESS units escalates, the computational complexity rises exponentially due to the corresponding increase in the number of constraints and binary variables. This escalation made the optimization problem much more challenging to solve and may take an impractically long time to obtain a feasible solution. Thus, the research gap lies in finding methods to reduce the computational burden associated with neural network integrated optimization problems.

Heuristic methods were proposed in reducing the complexity of neural network models. For instance, in [30], a low-complexity neural belief propagation decoder is constructed using network pruning techniques. This approach involves removing unimportant edges from the network structure. However, it should be noted that these techniques may inadvertently decrease the training accuracy. Another approach to reducing complexity is the utilization of a sparse feature learn-

ing model [31]. This model focuses on learning useful representations and decreasing the complexity of hierarchical deep neural network models. In [32], the effectiveness of sparse convolutional neural networks for single-instruction-multiple-data (SIMD)-like accelerators is demonstrated. This technique helps alleviate the computational burden by applying pruning methods to eliminate unnecessary connections within fully connected structures, as exemplified in [33] for wideband power amplifiers' neural network models. Similarly, pruning techniques are also employed in [34] to compact the deep neural networks for SCADA applications. Furthermore, [35]-[36] suggest that modern deep neural networks often suffer from overparameterization, with a large number of learnable parameters. One potential solution to this issue is model compression through the use of sparse connections. These approaches contribute to reducing the complexity and computational burden associated with neural network models, enabling more efficient and streamlined implementations.

Since the sparsity and pruning techniques have proved to be efficient to reduce the complexity of neural networks in many other applications, it may be a perfect solution to obtain a low computational complexity model in battery degradation prediction. Thus, we propose a sparse neural network-based battery degradation model (SNNBD) to quantify the battery degradation in BESS daily operations. SNNBD is designed to be significantly less complex than the traditional fully-connected dense neural network model. SNNBD is designed to reduce the computation burden induced by the ReLU activation function. Achieving this entails a strategic process of pruning during training, whereby a predetermined percentage of neurons is systematically pruned. The sparsity percentage is defined as the ratio of pruned neurons to the total neurons in the neural network. A higher percentage of sparsity may decrease the computation complexity significantly, but the accuracy of the battery degradation prediction may decrease as compared with a less-sparse or dense model. It will be a trade-off between the sparsity and the training accuracy. Compared to the NNBD model [29], the proposed SNNBD model contains only a percentage of NNBD's neurons which may reduce the computational burden significantly while maintaining accurate battery degradation prediction.

The main contributions of this paper are as follows:

- *Refined Battery Degradation Modeling*: The proposed SNNBD model significantly refines existing NNBD model, elevating its proficiency in quantifying battery degradation within the day-ahead scheduling model.
- *Computational Augmentation with SNNBD*: To efficiently address the day-ahead scheduling optimization challenge, this paper proposes an innovative SNNBD-assisted computational enhancement model. Capitalizing on the capabilities of the SNNBD model, this enhancement substantially improves the computational efficiency of the optimization process. This, in turn, translates into more responsive and informed decision-making procedures.
- *Linearization Technique for Practicality*: The integration of the SNNBD model into the day-ahead scheduling framework is accompanied by a pertinent linearization technique. This technique simplifies the model's analysis and evaluation, making it more practical and feasible for real-world application scenarios.

- *Versatile Performance Evaluation*: This paper showcases the SNNBD model's efficacy across various levels of sparsity, and highlights its adaptability in capturing battery degradation under diverse operational scenarios. The day-ahead scheduling, enriched by the SNNBD model, is rigorously assessed on both expansive bulk power systems and local microgrid systems. These validation trials substantiate the SNNBD model's robustness and effectiveness in real-world power system environments.
- *In-depth Economic Insights*: This paper provides an insightful market analysis. By comparing locational marginal prices (LMPs) across three scenarios: (1) zero-degradation BESS, (2) degraded BESS, and (3) no BESS integration, the economic implications and advantages of incorporating BESS into the power system and capturing its degradation are explored. This analysis provides a comprehension of the economic landscape, enriching decision-making processes within the energy market.

The rest of the paper is organized as follows. Section II describes the sparse neural network model and training strategy. Section III presents the traditional day-ahead scheduling model. Section IV presents the SNNBD integrated day-ahead scheduling model. Section V presents case studies and Section VI concludes the paper.

## II. SPARE NEURAL NETWORK BASED BATTERY DEGRADATION

This section outlines the training process for the proposed SNNBD model. We proposed two training schemes: (i) Warm Start that trains the SNNBD based on the pre-trained NNBD model, and (ii) Cold Start that trains the SNNBD model directly with random initial weights. Both models consist of 5 input neurons, 20 neurons in hidden layer 1, 10 neurons in hidden layer 2, and 1 neuron in the output layer. The hidden layers utilize the ReLU as the activation function for each neuron.

### A. Warm Start

The training process for Warm Start is illustrated in the algorithm explained below. Initially, the weights derived from the trained neural network model are utilized as the initial weights for the SNNBD model. During the training of the SNNBD model, a pruning mask is generated based on a certain predetermined sparsity percentage value. This mask is then applied to prune the weights after each training epoch to achieve the desired sparsity. The pruning masks are binary matrices that indicate which neurons are pruned (set to zero) in order to achieve sparsity throughout the entire structure.

---

#### Training Algorithm: Sparse Neural Network

---

1. Obtain the weights matrices  $\omega$  from the pre-trained NNBD model.
  2. Set the sparse percentage  $\epsilon$ .
  3. Set the training epochs.
  4. **For**  $e$  in epochs,
  5.     Set the Pruning masks matrices with the  $\epsilon$
  6.     Update weights matrices by  $\omega * \epsilon$
  7.     Tune the weights matrices with gradient descent.
  8. **end For**
- 

### B. Cold Start

Cold Start offers a simple approach compared to Warm Start. Instead of training the neural network based on the fine-tuned NNBD weights, Cold Start directly trains a sparse neural network using random initial weights. In essence, the key difference between Warm Start and Cold Start lies in the

choice of initial weights. However, all other training techniques remain consistent between the two options. The performance and efficiency of both Warm Start and Cold Start will be evaluated and compared the performance.

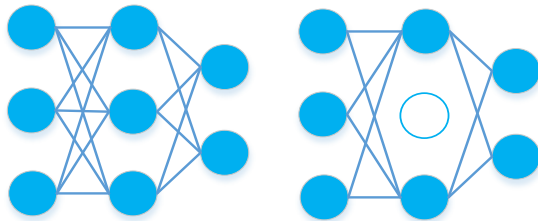
### C. NNBD Model

The training of deep neural networks requires a substantial amount of data. In our study, we utilize MATLAB Simulink [37] to perform battery aging tests by implementing a battery model. By employing a battery cycle generator, we simulate charging and discharging cycles at predefined rates and replicate various battery types, conditions, operating profiles, ambient temperature effects, and internal resistance. These battery aging tests are conducted at different initial SOC and DOD levels, as well as under different ambient temperatures and charging/discharging rates.

In order to enhance the training efficiency and accuracy of the model, the battery degradation data collected from Simulink needs to be normalized before being fed into the training process. The original data consists of SOC, DOD, temperature, charging/discharging rate, and SOH. The C Rate, denoting the speed at which a battery is charged or discharged. SOH data is collected at the end of each charging/discharging cycle when the battery returns to its pre-set SOC value. Each cycle represents the process of discharging a battery from a specific SOC to a lower SOC and then recharging it back to the original SOC.

### D. Pruning Method

Pruning is a technique employed in neural networks to reduce the size and complexity of a model by eliminating unnecessary connections or neurons [38]. The objective of pruning is to enhance the efficiency of the training model, minimize memory requirements, and potentially improve its generalization capabilities. During the pruning process, a pruning mask is applied to identify and eliminate neurons that contribute less to the overall network performance, as depicted in Fig. 1. The pruning masks are regenerated for each epoch which means each pruning mask are identical. It also helps the robustness of the proposed SNNBD model. These pruning masks enable a compact representation of the sparse neural network. Instead of storing and computing all connection weights, only the active connections are considered, resulting in reduced memory usage and computational demands. By incorporating pruning masks, sparse neural networks strike a balance between model complexity and efficiency, making them a valuable approach for various applications, particularly in scenarios with limited computational resources or deployment constraints.



Before Pruning                      After Pruning  
Fig. 1. Pruning of a sample neural network model.

### E. Fine Tuning and Setup

After the pruning stage, the network undergoes retraining to restore and fine-tune its performance in the next epoch. During retraining, the pruning mask plays a crucial role in removing the pruned connections, effectively fixing their weights at zero. Only the remaining active connections are updated during the retraining process. This allows the network to relearn and redistribute its capacity among the remaining connections, compensating for the pruned ones.

During the training phase, the sparse neural network is trained using the mini-batch gradient descent strategy. The performance of the deep neural network is assessed based on its capacity to make precise predictions, which is evaluated using the mean squared error metric as shown in equation (1). The mean squared error is computed by averaging the squared differences between the actual and predicted values across all the training data points, serving as the loss function throughout the training process.

$$\text{Mean Square Error} = \frac{1}{n} \sum_{i=1}^n (y_i - \tilde{y}_i)^2 \quad (1)$$

## III. TRADITIONAL DAY-AHEAD SCHEDULING MODEL

This section presents the day-ahead scheduling problem for both the bulk power system and the microgrid system. The bulk power system is inherently more complex than the microgrid system due to the presence of multiple buses and transmission lines. It's important to note that neither of the models listed in this section consider the battery degradation.

### A. Bulk Power System Energy Scheduling Model

The day-ahead scheduling problem of the bulk power system is represented by the traditional security constrained unit commitment (SCUC) model. The objective of the traditional SCUC model is to minimize the total operating cost of the system as defined in equation (2).

Objective function:

$$f^{\text{Cost}} = \sum_g \sum_t P_{g,t} c_{g,t} + U_g c_g^{\text{NL}} + V_g c_g^{\text{SU}}, \forall g, t \quad (2)$$

Constraints:

$$\sum_{g \in S_G} P_{g,t} + \sum_{wt \in S_{WT}} P_{wt,t} + \sum_{pv \in S_{PV}} P_{pv,t} + \sum_{s \in S_S} P_{s,t}^{\text{Disc}} + \sum_{k \in S_{n-}} P_{k,t} \quad (3)$$

$$= \sum_{k \in S_{n+}} P_{k,t} \sum_{l \in S_L} P_{l,t} + \sum_{s \in S_S} P_{s,t}^{\text{Char}} \quad (4)$$

$$P_g^{\text{Min}} \leq P_{g,t} \leq P_g^{\text{Max}}, \forall g, t \quad (4)$$

$$P_{g,t+1} - P_{g,t} \leq \Delta T \cdot P_g^{\text{Ramp}}, \forall g, t \quad (5)$$

$$P_{g,t} - P_{g,t+1} \leq \Delta T \cdot P_g^{\text{Ramp}}, \forall g, t \quad (6)$$

$$V_{g,t} \geq U_{g,t} - U_{g,t-1}, \forall g, t, \quad (7)$$

$$V_{g,t+1} \leq 1 - U_{g,t}, \forall g, t, \quad (8)$$

$$V_{g,t} \leq U_{g,t}, \forall g, t, \quad (9)$$

$$-P_k^{\text{Max}} \leq P_{k,t} \leq P_k^{\text{Max}}, \forall k, t, \quad (10)$$

$$P_{k,t} - b_k (\theta_{n(k)}^t - \theta_{m(k)}^t) = 0, \forall k, t, \quad (11)$$

$$U_{s,t}^{\text{Disc}} + U_{s,t}^{\text{Char}} \leq 1, \forall s, t \quad (12)$$

$$U_{s,t}^{\text{Char}} \cdot P_s^{\text{Min}} \leq P_{s,t}^{\text{Char}} \leq U_{s,t}^{\text{Char}} \cdot P_s^{\text{Max}}, \forall s, t \quad (13)$$

$$U_{s,t}^{\text{Disc}} \cdot P_s^{\text{Min}} \leq P_{s,t}^{\text{Disc}} \leq U_{s,t}^{\text{Disc}} \cdot P_s^{\text{Max}}, \forall s, t \quad (14)$$

$$E_{s,t} - E_{s,t-1} + \Delta T (P_{s,t-1}^{Disc} / \eta_s^{Disc} - P_{s,t-1}^{Char} \eta_s^{Char}) = 0, \forall s, t \quad (15)$$

$$E_{s,t=24} = E_s^{Initial}, \forall s \quad (16)$$

$$0 \leq E_{s,t} \leq E_{s,t}^{max} \quad (17)$$

The power balance equation for bus  $n$  incorporates synchronous generators, renewable energy sources, battery energy storage systems, and load demand, as represented by equation (3). Constraints (4-6) define the power output limits and ramping limits for each generator. To establish the relationship between a generator's start-up status and its on/off status, equations (7)-(9) are employed. Equation (10) enforces the thermal limit of the transmission lines. Constraint (11) calculates the power flow within the network.

For the BESS, the state of charge (SOC) level is determined by the ratio between the current stored energy and the maximum available energy capacity, as shown in equation (12). Constraints (13)-(14) maintain the charging/discharging power of the BESS within specified limits. Equation (15) calculates the stored energy of the BESS for each time interval. Equation (16) mandates that the final SOC level of the BESS matches the initial value. Equation (17) establishes the upper limit for the stored energy of the BESS.

### B. Microgrid Energy Scheduling Model

The traditional microgrid day-ahead scheduling problem shares some constraints of the bulk power system model, excluding the power flow constraints. The objective function for microgrids aims to minimize the total cost, incorporating the cost of traditional generators and the cost of tie-line power exchange, as depicted in (18).

#### Objective function:

$$f^{Cost} = \sum \sum (P_{g,t} c_{g,t} + U_g c_g^{NL} + V_g c_g^{SU}) + P_t^{Buy} c_t^{Buy} - P_t^{Sell} c_t^{Sell}, \forall g, t \quad (18)$$

#### Constraints:

The power balance equation for microgrid is presented in (19). To ensure the appropriate status of power exchange between the microgrid and the main grid, (20) is utilized, specifying the status of being a buyer, seller, or idle. Constraints (21) and (22) limit the thermal limits of the tie-line. Lastly, equation (23) setup the emergency reserve of the system. The traditional microgrid day-ahead scheduling constraints encompass (4)-(9) and (12)-(23). Unlike the power flow constraints present in the bulk power system model, the microgrid model incorporates tie-line exchange equations within the day-ahead scheduling framework.

$$P_t^{Buy} + \sum_{g \in S_G} P_{g,t} + \sum_{wt \in S_{WT}} P_{wt,t} + \sum_{pv \in S_{PV}} P_{pv,t} + \sum_{s \in S_S} P_{s,t}^{Disc} = P_t^{Sell} + \sum_{l \in S_L} P_{l,t} + \sum_{s \in S_S} P_{s,t}^{Char} \quad (19)$$

$$U_t^{Buy} + U_t^{Sell} \leq 1, \forall t \quad (20)$$

$$0 \leq P_t^{Buy} \leq U_t^{Buy} \cdot P_{Grid}^{Max}, \forall t \quad (21)$$

$$0 \leq P_t^{Sell} \leq U_t^{Sell} \cdot P_{Grid}^{Max}, \forall t \quad (22)$$

$$P_{Grid}^{Max} - P_t^{Buy} + P_t^{Sell} + \sum_{g \in S_G} (P_g^{Max} - P_{g,t}) \geq R_{percent} \left( \sum_{l \in S_L} P_{l,t} \right), \forall t \quad (23)$$

## IV. BATTERY DEGRADATION CONSIDERED DAY-AHEAD SCHEDULING MODEL

### A. Neural Network Based Battery Degradation Quantification

The battery degradation quantification is achieved by the SNNBD model. In this model, various variables of the BESS are processed and fed into the SNNBD model to predict the battery degradation per cycle of BESS operation. The input variables for the SNNBD model consist of temperature, SOC, DOD, C rate, and SOH. To calculate the DOD and C rate, (24) and (25) are utilized. Equation (26) predicts the battery degradation value, while (27) provides the equivalent degradation cost. In these equations,  $c_{BESS}^{Capital}$  represents the capital investment cost of the BESS,  $c_{BESS}^{SV}$  denotes the salvage value of the BESS, and  $SOH_{EOL}$  signifies the state of health value considered as the end of battery life.

Consequently, the equivalent battery degradation cost is included as an additional component in the objective functions of traditional models. To model the day-ahead scheduling considering battery degradation, constraints (24)-(27) are added to the traditional day-ahead scheduling model. However, solving this battery degradation model directly is challenging due to the highly non-linear nature of the ReLU activation function used in the neural network.

$$\Delta DOD_t = |SOC_t - SOC_{t-1}| \quad (24)$$

$$C_t^{Rate} = \Delta DOD_t / \Delta T \quad (25)$$

$$BD = \sum_t SNNBD(Variables) \quad (26)$$

$$f^{BESS} = \frac{c_{BESS}^{Capital} - c_{BESS}^{SV}}{1 - SOH_{EOL}} BD \quad (27)$$

### B. Piecewise-Linearization of SNNBD Model

The SNNBD model is characterized by a series of equations that describe the calculation and activation processes of neurons. Each neuron's computation is defined by (28), which takes into account the input features from the first layer, the corresponding weight matrix  $W$ , and the biases matrix. The activation function is employed in the SNNBD model, as shown in (29). This activation function is commonly used in neural networks to introduce non-linearity and capture complex relationships between variables. However, the non-linearity of the ReLU function can pose challenges when it is embedded in the optimization problem. To address this issue, the ReLU activation function can be linearized using an auxiliary binary variable, denoted as  $\delta_h^i$ . This variable is further defined in (30)-(33). Specifically,  $\delta_h^i$  takes a value of one when activation is enabled, meaning the input value is positive, and zero otherwise. The activated value of  $x_h^i$ , denoted as  $a_h^i$ , represents the output of the neuron after the ReLU activation is applied.

$$x_h^i = \sum x_{h-1}^i * W + Bias \quad (28)$$

$$a_h^i = \text{relu}(x_h^i) = \max(0, x_h^i) \quad (29)$$

$$a_h^i \leq x_h^i + \text{BigM} * (1 - \delta_h^i) \quad (30)$$

$$a_h^i \geq x_h^i \quad (31)$$

$$a_h^i \leq \text{BigM} * \delta_h^i \quad (32)$$

$$a_h^i \geq 0 \quad (33)$$

The SNNBD-integrated day-ahead energy scheduling models for different systems are shown in the Table I.

Systems	Equations
Bulk Power Grid	(2)-(17), (24)-(33)
Microgrid	(4)-(9), (12)-(33)

### C. Benchmark Model

To evaluate the performance of the SNNBD model in day-ahead scheduling problems, a benchmark model will be employed. The benchmark model utilizes the NNBD model, which has been previously introduced in studies. The purpose of this benchmark model is to provide a basis for comparison and assess the effectiveness of the SNNBD model.

It is important to note that there the day-ahead scheduling modeling remains consistent across both the NNBD and SNNBD models. Both models are applied within the same day-ahead scheduling framework, sharing the same variables and constraints. The distinction between the two models lies in the methodology used to quantify battery degradation. The NNBD model, used in the benchmark model, employs a conventional deep neural network approach to predict battery degradation based on the input variables. In contrast, the SNNBD model, under evaluation, utilizes a sparse neural network architecture. By comparing the performance of the SNNBD model against the benchmark NNBD model, it becomes possible to evaluate the effectiveness of the sparse architecture introduced in the SNNBD model. This comparison aids in determining the advancements made by the SNNBD model in compact the neural network structure, which in turn can contribute to reduce the computational complexity of the neural network integrated day-ahead scheduling problems.

## V. CASE STUDIES

### A. Training Strategies: Warm Start vs. Cold Start

The analysis of training outcomes, as illustrated in Table II, distinctly highlights the superiority of Warm Start over Cold Start concerning training accuracy. However, it's noteworthy that Cold Start requires fewer epochs to complete the training process. It is important to mention that the training epochs for Warm Start represent the combined training epochs required by the NNBD model and the SNNBD model, while for Cold Start, it refers to the training epochs of the sparse neural network alone. Training the sparse neural network from random initial weights (Cold Start) proves to be notably challenging when it comes to achieve an equivalently level of accuracy as the Warm Start. In contrast, Warm Start is designed to take advantage of the pre-trained NNBD model, which serves as a stable starting point. The SNNBD model is then applied to further refine and sparse the structure of the already trained model. This suggests that the pre-trained NNBD model provides a beneficial foundation for the SNNBD model. The initial training with the NNBD model establishes a solid baseline, and the subsequent application of the SNNBD model

enables fine-tuning with sparsity. By leveraging the existing knowledge encoded in the NNBD model, Warm Start demonstrates superior training accuracy compared to Cold Start.

Table II Results between Warm Start and Cold Start

Training Options	Accuracy	Epochs
Warm Start	94%	550
Cold Start	77%	300

### B. SNNBD Model Training

All the results presented here are based on training Warm Start, as it outperforms the Cold Start. The training results of the proposed SNNBD model are depicted in Fig. 2 and Table III. In Fig. 2, the 0% sparsity represents the original NNBD model without any sparsity applied. The subsequent markers—5%, 10%, and 15%—tinted in blue, red, and green, respectively, signify distinct error tolerance thresholds. Notably, the pattern that unfolds the interplay between sparsity and prediction accuracy. As sparsity percentage scales up, the precision of battery degradation value predictions undergoes a gradual decrement across all tolerance thresholds. This trend continues until the 70% sparsity mark is attained. When comparing the 0% sparsity model (NNBD model) and the 50% sparsity model, the accuracy stands at 94.5% and 93.7% respectively, considering a 15% error tolerance. However, the 50% sparsity model significantly reduces the computational complexity compared to the original NNBD model since half of the neurons are pruned to be zero, thereby eliminating their connections. This reduction in computational complexity is exponential, as all connections associated with zero-valued neurons are discarded.

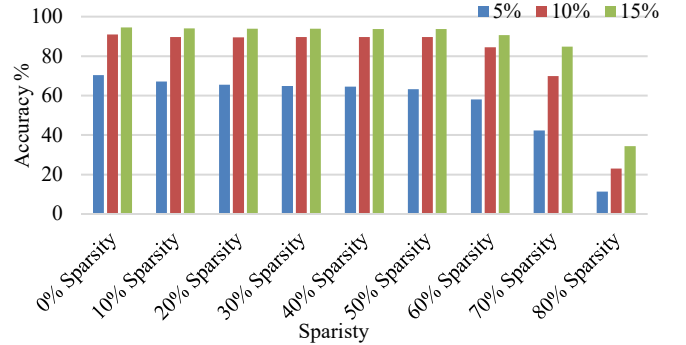


Fig. 2. Training results of SNNBD model at different sparsity levels.

Table III. Training accuracies of proposed SNNBD model under different sparsity levels and error tolerances

Sparsity Percentage	Error Tolerances		
	5%	10%	15%
0%	70%	91%	95%
10%	67%	90%	94%
20%	66%	90%	94%
30%	65%	90%	94%
40%	65%	90%	94%
50%	63%	90%	94%
60%	58%	84%	91%
70%	42%	70%	85%
80%	11%	23%	34%

All of these models, including the original NNBD model and models with various sparsity levels, will be integrated into the day-ahead scheduling problem to evaluate their performance. This integration will provide further validation and enable the evaluation of their effectiveness in improving the overall optimization process in the day-ahead scheduling problem.

### C. Microgrid Test Case

To evaluate the performance of the integrated SNNBD day-ahead scheduling model, a typical grid-connected microgrid with renewable energy sources was employed as a testbed, as demonstrated in Section IV. The microgrid configuration consists of several components, including a traditional diesel generator, wind turbines, residential houses equipped with solar panels, and a lithium-ion BESS with a charging/discharging efficiency of 90%. The parameters for these main components are provided in Table IV.

To simulate realistic conditions, the load data for the microgrid is based on the electricity consumption of 1000 residential houses. The ambient temperature and available solar power for a 24-hour period are sourced from the Pecan Street Dataport [39], ensuring accurate representation of real-world environmental conditions. The wholesale electricity price data is obtained from ERCOT [40], allowing the model to consider market dynamics in the day-ahead scheduling decisions.

The optimization problem, formulated as part of the day-ahead scheduling model, was solved on a computer with the following specifications: an AMD® Ryzen 7 3800X processor, 32 GB RAM, and an Nvidia Quadro RTX 2700 Super GPU with 8 GB of memory. The Pyomo [41] package, a powerful optimization modeling framework, was utilized to formulate and solve the day-ahead optimization problem. A high-performance mathematical programming solver Gurobi [42] was employed to efficiently find optimal solutions. By utilizing this realistic microgrid test platform and the computational resources mentioned, the SNNBD integrated day-ahead scheduling model can accurately capture the dynamics of the renewable energy sources, optimize the scheduling decisions, and assess the performance of the proposed approach.

Table IV. Microgrid testbed

Main Components	Diesel Generator	Wind Turbines	Solar Panels	Lithium-ion BESS
Size	180kW	1000kW	1500kW	300kWh

Table V presents the validation results for different sparsity levels of the SNNBD models in the microgrid day-ahead scheduling problem. The table provides insights into the performance of these models across various metrics. "Pseudo Total" represents the total cost with the SNNBD model, which serves as the objective of the day-ahead scheduling including the operating cost and degradation cost in optimization problem. "BD Cost" represents the equivalent battery degradation cost estimated using the SNNBD model. "Operation" shows the microgrid operating cost, including the cost associated with generators and power trading. "OG BD Cost" indicates the battery degradation cost obtained from the original NNBD model, which does not incorporate sparsity. "Updated Total" represents the sum of the operation cost and the "OG BD Cost". "0% sparsity" is considered as the benchmark model, used to evaluate the performance of the other SNNBD models with different sparsity levels.

From the information in Table V, it appears that the SNNBD model does not significantly reduce the solving time in the microgrid model. Furthermore, there is no substantial difference observed in the total cost and updated total cost among the various SNNBD models compared to the benchmark model. These findings suggest that the inclusion of sparsity in the SNNBD model does not significantly impact the

overall cost in the microgrid day-ahead scheduling problem. Fig. 3 illustrates the output curves of the BESS under different battery degradation models. The figure shows that the BESS charge/discharge power profiles largely overlap across most time intervals. The only notable difference is observed in the 10% and 20% sparsity models, where the BESS charges at 20 kW during the 7-8 pm. Overall, these results demonstrate that the SNNBD model is capable of finding solutions for the day-ahead scheduling problem. Based on these findings, it can be concluded that the SNNBD model is reliable and able to identify optimal solutions compared to the non-sparse NNBD model in the microgrid day-ahead scheduling problem. However, it should be noted that the SNNBD model does not yield efficiency improvements, even with higher sparsity levels. One possible reason for this observation could be the small scale of the microgrid case and the presence of only one BESS, which does not impose a heavy computational burden.

Table V. Microgrid energy scheduling results

Sparsity	0%	10%	20%	30%	40%
Pseudo Total (\$)	501.5	499.94	500.88	501.2	501.04
BD Cost (\$)	7.27	7.93	8.85	7.4	8.22
Operation (\$)	494.23	492.01	492.03	493.8	492.82
OG BD Cost (\$)	7.27	11.25	11.2	8.09	9.27
Updated Total (\$)	501.5	503.26	503.23	501.89	502.09
Solving time (s)	8.39	4.99	9	6.73	6.72

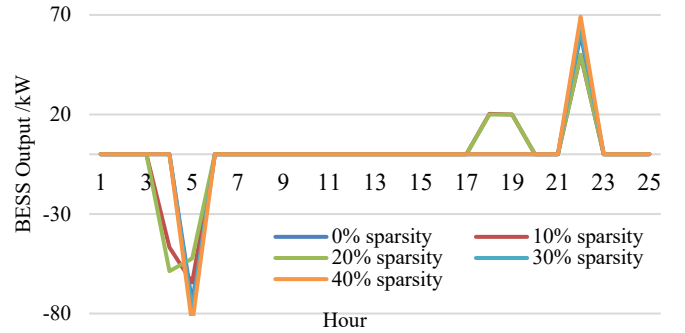


Fig. 3. BESS output in a microgrid system.

### D. Bulk Power System Test Case

To evaluate the day-ahead scheduling of the bulk power grid model, a typical IEEE 24-bus system (Fig. 4) [43] is employed as a test bed. This system consists of 33 generators and serves as a representative model for large-scale power grids. In addition to the existing infrastructure, the test bed incorporates several BESSs and wind farms to evaluate their impact on the day-ahead scheduling. Fig. 4 illustrates the layout of the IEEE 24-bus system, showcasing the interconnected buses and the corresponding transmission lines. The objective of this evaluation is to optimize the scheduling decisions considering the presence of the multiple BESS and wind farm within the larger power grid system.

Similar to the microgrid case discussed earlier, the day-ahead scheduling problem for the bulk power grid is solved using same solving software packages. The integration of the BESS and wind farm within the IEEE 24-bus system enables the evaluation of their impact on optimizing power generation, transmission, and scheduling decisions at a larger scale.

Table VI provides the parameters of the BESSs installed at different buses within the IEEE 24-bus system. These parameters characterize the specifications of each BESS, including

their energy capacities and power output capabilities. Notably, BESS number four possesses the largest energy capacity and the highest output power among the five BESSs considered in the system. The minimum power for charging or discharging is set to zero. Additionally, the IEEE 24-bus system incorporates five wind farms, each comprising a varying number of wind turbines. The capacity of each wind turbine is fixed at 200 kW. To obtain suitable wind profiles for this study, the wind profile data sourced from the Pecan Street Dataport [41] are appropriately scaled. The inclusion of these parameters and data in the evaluation allows for a comprehensive analysis of the day-ahead scheduling problem within the IEEE 24-bus system.

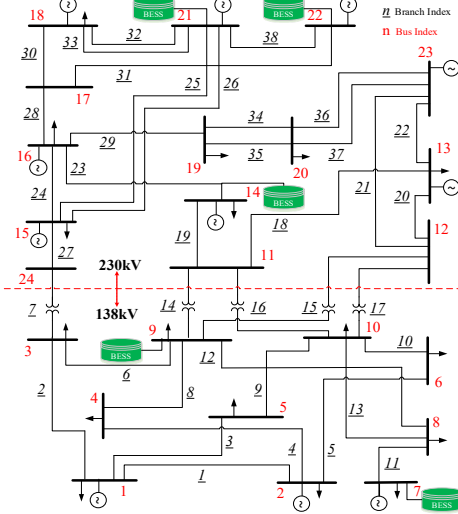


Fig. 4. Illustration of the modified IEEE 24-bus system [43].

Table VI Setting of BESSs

BESS No.	Bus No.	Energy Capacity (MWh)	Power Rating (MW)	Initial SOC
1	21	50	20	40%
2	22	10	4	40%
3	7	10	4	40%
4	14	200	100	40%
5	9	30	10	50%

The outcome for the IEEE 24-bus system with different sparsity levels of the SNNBD model are presented in Table VII. It is vital to recognize that all tabulated results are anchored on a relative MipGap of 0.001, which is a critical gauge of the optimality gap. The table clearly demonstrates that the solving time decreases exponentially as the sparsity level of the SNNBD model. The results based on the 60% and 70% sparsity have not been included as the BESS output curve deviates significantly from the solutions based on lower sparsity level models. The 0% and 10% sparsity models results are not listed here since they cannot be solved within the given time frame, whereas the 50% sparsity model requires only 455 seconds for solution. Similarly, for the 20% sparsity model, the day-ahead scheduling problem cannot find the optimal solution within the span of 20 hours, resulting in a reported non-optimal benchmark result.

We also found that the 50% sparsity model lead to the minimum total cost. However, the total cost, does not change significantly despite the variation in solving time. This indicates that while the solving time is reduced to an acceptable number with high sparsity SNNBD models, the overall cost remains

relatively stable. By analyzing these results, it becomes evident that increasing the sparsity level in the SNNBD model significantly reduces solving time without significantly impacting the overall cost. However, it is crucial to validate the BESS power output pattern when assessing the performance of the SNNBD model. Examining the BESS power output pattern ensures that the model captures the desired behavior and produces outputs consistent with expectations.

Figs. 5 and 6 display the SOC curves of BESS #4 and #5 under different sparsity levels of the proposed SNNBD model. These two BESS units are particularly active among the five units considered in the testbed. For benchmarking purposes, the SOC curve is also plotted when there is no battery degradation considered in the day-ahead scheduling problem. The SOC curve provides insights into the utilization of the BESS, with more fluctuation indicating more active and flatter curves indicating less active. When degradation is not considered, the BESS units are utilized to their maximum capacity since there is no equivalent degradation cost factored into the optimization problem. We found that both BESS #4 and #5 are scheduled to discharge to 0% SOC twice when degradation is not considered. In Figure 5, the output curves of BESS #4 with SNNBD models significantly shrink compared to the case where degradation is not considered. However, the output patterns of BESS #4 with different sparsity levels of the SNNBD model exhibit a similar pattern and overlap for most time periods, which demonstrating the effectiveness of the proposed SNNBD model.

Table VII IEEE 24 bus day-ahead scheduling results based on different SNNBD models

Sparsity Percentage	Operation Cost (\$)	Degradation Cost (\$)	Updated Total (\$)	Time (s)
20%	259,435	9,933	269,368	72,000
30%	259,848	10,447	270,295	4,383
40%	260,186	9,806	269,992	1,858
50%	259,472	6,789	266,261	455

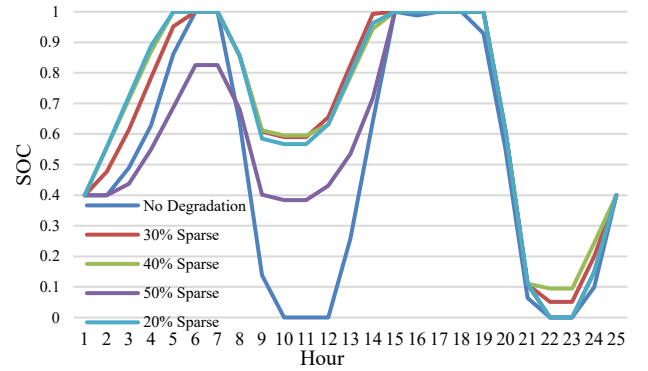


Fig. 5. SOC curves of BESS #4 in the 24-bus bulk power system.

The output patterns of BESS #5 in Figure 6 appear different from those of BESS #4. However, similar to BESS #4, BESS #5 discharges significantly less when degradation is considered. Table III provides insights into the tradeoff between sparsity and accuracy. A higher sparsity level leads to lower accuracy, while a lower sparsity level results in longer solving times for day-ahead scheduling. Thus, a balance must be compromised between sparsity and accuracy. Overall, the 50% sparsity model performs the best since its SOC curve closely resembles those of the 20%, 30%, and 40% sparsity models while having the lowest total cost.

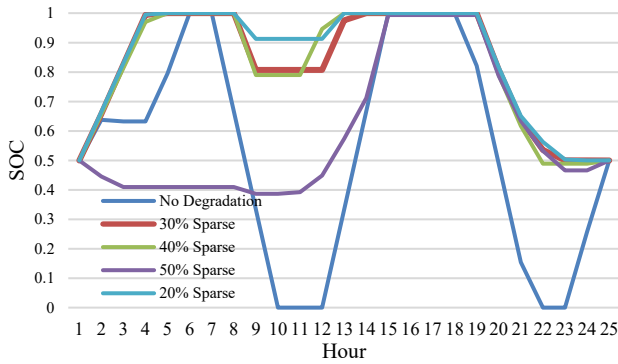


Fig. 6. SOC curves of BESS #5 in the 24-bus bulk power system.

### E. Market Analysis

Fig. 7 presents sample results demonstrating the influence of locational marginal price (LMP) when integrating BESSs into the bulk power system. Our exploration encompassed 3 models including “no BESS model”, “BESS considered with degradation”, and “BESS considered without degradation”. A comparison was made with the “no BESS model” to assess the system’s ability to reduce line congestion when a BESS is integrated. The LMP results in Fig. 7 specifically focus on bus 14, the location of the largest BESS unit, BESS #4. From the figure, it is evident that during most time periods, such as 1 am to 5 am and 12 pm to 6 pm, the LMP values are consistent across the different cases, indicating there is no line congestion at bus 14 during those periods. However, as the clock strikes 3 pm to 6 pm, a surge in LMP is evident, which suggests that the line is loaded higher than in the previous hours but is not yet congested. During the normal daily peak load periods of 7 am to 9 am and 7 pm to 8 pm, the LMP values differ among the proposed models. In comparison to the “no BESS model,” the models with integrated BESS units can significantly reduce the LMP, indicating that the BESS can alleviate line congestion. Note that when battery degradation is not considered, the BESS exhibits a higher capability to mitigate line congestion, leading to the lowest LMP during those congested hours. This analysis of LMP with the integration of a BESS system provides valuable insights for both grid operators and BESS investors, as BESS installations play a crucial role in addressing line congestion within the grid.

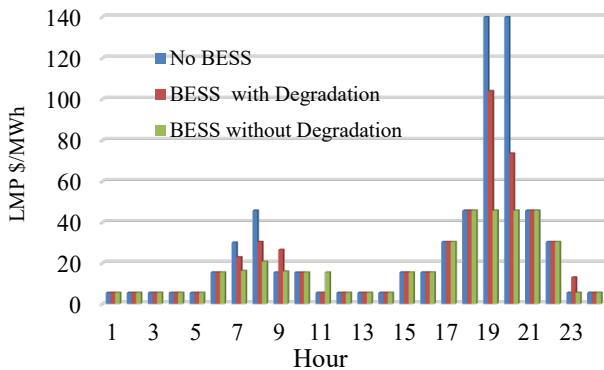


Fig. 7. LMP at bus 14 (BESS #4).

### F. Sensitivity Analysis of Relative Optimization Gaps

A sensitivity test was conducted to examine the impact of different relative gaps. Fig. 8 displays SOC curves of BESS #4 based on the optimal solution obtained using different relative MipGap values. The results presented in Figure 8 are based on

the 50% sparsity SNNBD model. The solving times for MipGap values of 0.01, 0.005, and 0.001 are 339 seconds, 380 seconds, and 450 seconds, respectively. The solving time increases as the MipGap value decreases because a more accurate optimal solution is sought. However, upon analyzing the SOC curve depicted in Figure 8, it becomes evident that the SOC curves mostly overlap, indicating minimal differences between the solutions obtained under different MipGap values. Consequently, for the 50% sparsity model, a higher MipGap value is preferred as it reduces the computation time while maintaining a comparable solution quality.

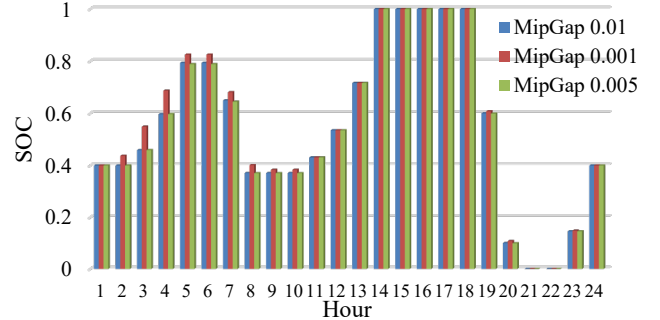


Fig. 8. Scheduled SOC levels of BESS #4 at bus 14.

## VI. CONCLUSIONS

This paper introduces a novel sparse neural network-based battery degradation model that can accurately quantify battery degradation in BESS and largely address the computational challenges associated with traditional dense neural networks when being incorporated into optimization models. By leveraging the sparse technique, the proposed SNNBD achieves accurate degradation prediction while significantly reducing the computational complexity. It has been proven that the accuracy of the SNNBD model does not decrease significantly until the sparsity is increased to 80%. It can obtain 91% accuracy at 60% sparsity, compared to 95% when no sparsity is implemented.

The results also show that our proposed SNNBD model can significantly reduce the computational burden, making neural network-integrated day-ahead energy scheduling directly solvable, even for complicated multi-BESS integrated systems. Furthermore, the results have been proven to be accurate and feasible with a high sparsity SNNBD model in both microgrid and bulk power system. Choosing different sparsity levels for the proposed SNNBD model provides flexibility for the grid operator, as it involves a tradeoff between accuracy and solving time. Overall, the SNNBD model opens up new possibilities for efficiently addressing battery degradation in day-ahead energy scheduling for multi-BESS systems.

## REFERENCES

- [1] T. Mai et al., “Renewable Electricity Futures for the United States,” in *IEEE Transactions on Sustainable Energy*, vol. 5, no. 2, pp. 372–378, April 2014.
- [2] B. Li, T. Chen, X. Wang and G. Giannakis, “Real-Time Energy Management in Microgrids With Reduced Battery Capacity Requirements,” *IEEE Trans. Smart Grid.*, vol. 10, no. 2, pp. 1928–1938, Mar. 2019.
- [3] X. Gong, R. Xiong and C. C. Mi, “Study of the Characteristics of Battery Packs in Electric Vehicles With Parallel-Connected Lithium-Ion Battery Cells,” in *IEEE Transactions on Industry Applications*, vol. 51, no. 2, pp. 1872–1879, March-April 2015.

- [4] A. M. Abomazid, N. A. El-Taweel and H. E. Z. Farag, "Optimal Energy Management of Hydrogen Energy Facility Using Integrated Battery Energy Storage and Solar Photovoltaic Systems," in *IEEE Transactions on Sustainable Energy*, vol. 13, no. 3, pp. 1457-1468
- [5] M. H. Nehrir et al., "A Review of Hybrid Renewable/Alternative Energy Systems for Electric Power Generation: Configurations, Control, and Applications," in *IEEE Transactions on Sustainable Energy*, vol. 2, no. 4, pp. 392-403, Oct. 2011.
- [6] M. T. Lawder et al., "Battery Energy Storage System (BESS) and Battery Management System (BMS) for Grid-Scale Applications," in *Proceedings of the IEEE*, vol. 102, no. 6, pp. 1014-1030, June 2014.
- [7] X. Gong, R. Xiong and C. C. Mi, "Study of the Characteristics of Battery Packs in Electric Vehicles With Parallel-Connected Lithium-Ion Battery Cells," in *IEEE Transactions on Industry Applications*, vol. 51, no. 2, pp. 1872-1879, March-April 2015.
- [8] A. Merabet, K. Tawfique Ahmed, H. Ibrahim, R. Beguenane and A. M. Y. M. Ghias, "Energy Management and Control System for Laboratory Scale Microgrid Based Wind-PV-Battery," in *IEEE Transactions on Sustainable Energy*, vol. 8, no. 1, pp. 145-154, Jan. 2017.
- [9] C. Zhao and X. Li, "A Novel Real-Time Energy Management Strategy for Grid-Friendly Microgrid: Harnessing Internal Fluctuation Internally," *52nd North American Power Symposium*, (Virtually), Tempe, AZ, USA Apr. 2021.
- [10] C. Zhao and X. Li, "A Novel Real-Time Energy Management Strategy for Grid-Supporting Microgrid: Enabling Flexible Trading Power," *IEEE PES General Meeting*, (Virtually), Washington D.C., USA, Jul. 2021.
- [11] P. S. Kumar, R. P. S. Chandrasena, V. Ramu, G. N. Srinivas and K. V. S. M. Babu, "Energy Management System for Small Scale Hybrid Wind Solar Battery Based Microgrid," in *IEEE Access*, vol. 8, pp. 8336-8345, 2020.
- [12] C. Zhao and X. Li, "A 100% Renewable Energy System: Enabling Zero CO2 Emission Offshore Platforms," *54th North American Power Symposium*, Salt Lake City, UT, USA, pp. 1-5, Oct. 2022.
- [13] A. Merabet, K. Tawfique Ahmed, H. Ibrahim, R. Beguenane and A. M. Y. M. Ghias, "Energy Management and Control System for Laboratory Scale Microgrid Based Wind-PV-Battery," in *IEEE Transactions on Sustainable Energy*, vol. 8, no. 1, pp. 145-154, Jan. 2017.
- [14] X. Xing, L. Xie, H. Meng, X. Guo, L. Yue and J. M. Guerrero, "Energy management strategy considering multi-time-scale operational modes of batteries for the grid-connected microgrids community," in *CSEE Journal of Power and Energy Systems*, vol. 6, no. 1, pp. 111-121, March 2020.
- [15] Z. Miao, L. Xu, V. R. Disfani and L. Fan, "An SOC-Based Battery Management System for Microgrids," in *IEEE Transactions on Smart Grid*, vol. 5, no. 2, pp. 966-973, March 2014.
- [16] B. Li, T. Chen, X. Wang and G. B. Giannakis, "Real-Time Energy Management in Microgrids With Reduced Battery Capacity Requirements," in *IEEE Transactions on Smart Grid*, vol. 10, no. 2, pp. 1928-1938, March 2019.
- [17] Y. Zhang, R. Xiong, H. He and M. G. Pecht, "Long Short-Term Memory Recurrent Neural Network for Remaining Useful Life Prediction of Lithium-Ion Batteries," in *IEEE Transactions on Vehicular Technology*, vol. 67, no. 7, pp. 5695-5705, July 2018.
- [18] B. Xu, A. Oudalov, A. Ulbig, G. Andersson and D. S. Kirschen, "Modeling of Lithium-Ion Battery Degradation for Cell Life Assessment," in *IEEE Transactions on Smart Grid*, vol. 9, no. 2, pp. 1131-1140, March 2018.
- [19] Z. Lyu, R. Gao, and L. Chen, "Li-Ion Battery State of Health Estimation and Remaining Useful Life Prediction Through a Model-Data-Fusion Method," *IEEE TRANSACTIONS ON POWER ELECTRONICS*, vol. 36, no. 6, pp. 6228-6240, June. 2021.
- [20] X. Han, L. Lu, Y. Zheng, X. Feng, Z. Li, J. Li, M. Ouyang, "A review of the key issues of the lithium ion battery degradation among the whole life cycle", in *eTransportation*, vol 1, Jul. 2019.
- [21] M. A. Hannan, M. M. Hoque, A. Hussain, Y. Yusof and P. J. Ker, "State-of-the-Art and Energy Management System of Lithium-Ion Batteries in Electric Vehicle Applications: Issues and Recommendations," in *IEEE Access*, vol. 6, pp. 19362-19378, 2018.
- [22] A. El Mejdoubi, H. Chaoui, H. Gualous, P. Van Den Bossche, N. Omar and J. Van Mierlo, "Lithium-Ion Batteries Health Prognosis Considering Aging Conditions," in *IEEE Transactions on Power Electronics*, vol. 34, no. 7, pp. 6834-6844, July 2019.
- [23] J. -O. Lee, Y. -S. Kim, T. -H. Kim and S. -I. Moon, "Novel Droop Control of Battery Energy Storage Systems Based on Battery Degradation Cost in Islanded DC Microgrids," in *IEEE Access*, vol. 8, pp. 119337-119345, 2020.
- [24] S. Fang, B. Gou, Y. Wang, Y. Xu, C. Shang and H. Wang, "Optimal Hierarchical Management of Shipboard Multibattery Energy Storage System Using a Data-Driven Degradation Model," in *IEEE Transactions on Transportation Electrification*, vol. 5, no. 4, pp. 1306-1318, Dec. 2019.
- [25] M. Chen, Z. Liang, Z. Cheng, J. Zhao and Z. Tian, "Optimal Scheduling of FTPSS With PV and HESS Considering the Online Degradation of Battery Capacity," in *IEEE Transactions on Transportation Electrification*, vol. 8, no. 1, pp. 936-947.
- [26] C. Ju, P. Wang, L. Goel and Y. Xu, "A Two-Layer Energy Management System for Microgrids With Hybrid Energy Storage Considering Degradation Costs," in *IEEE Transactions on Smart Grid*, vol. 9, no. 6, pp. 6047-6057, Nov. 2018.
- [27] L. Zhang et al., "Improved Cycle Aging Cost Model for Battery Energy Storage Systems Considering More Accurate Battery Life Degradation," in *IEEE Access*, vol. 10, pp. 297-307, 2022.
- [28] G. He, S. Kar, J. Mohammadi, P. Moutis and J. F. Whitacre, "Power System Dispatch With Marginal Degradation Cost of Battery Storage," in *IEEE Transactions on Power Systems*, vol. 36, no. 4, pp. 3552-3562, July 2021.
- [29] C. Zhao and X. Li, "Microgrid Optimal Energy Scheduling Considering Neural Network based Battery Degradation," *IEEE Transactions on Power Systems*, early access, Jan. 2023.
- [30] S. Han and J. Ha, "A Low-complexity Neural BP Decoder with Network Pruning," *2020 International Conference on Information and Communication Technology Convergence (ICTC)*, Jeju, Korea (South), 2020, pp. 1098-1100.
- [31] M. Gong, J. Liu, H. Li, Q. Cai and L. Su, "A Multiobjective Sparse Feature Learning Model for Deep Neural Networks," in *IEEE Transactions on Neural Networks and Learning Systems*, vol. 26, no. 12, pp. 3263-3277, Dec. 2015.
- [32] B. -C. Lai, J. -W. Pan and C. -Y. Lin, "Enhancing Utilization of SIMD-Like Accelerator for Sparse Convolutional Neural Networks," in *IEEE Transactions on Very Large Scale Integration (VLSI) Systems*, vol. 27, no. 5, pp. 1218-1222, May 2019.
- [33] Z. Liu, X. Hu, L. Xu, W. Wang and F. M. Ghannouchi, "Low Computational Complexity Digital Predistortion Based on Convolutional Neural Network for Wideband Power Amplifiers," in *IEEE Transactions on Circuits and Systems II: Express Briefs*, vol. 69, no. 3, pp. 1702-1706, March 2022.
- [34] A. Ashiqzaman, L. V. Ma, S. Kim, D. Lee, T. -W. Um and J. Kim, "Compacting Deep Neural Networks for Light Weight IoT & SCADA Based Applications with Node Pruning," *2019 International Conference on Artificial Intelligence in Information and Communication (ICAIIIC)*, Okinawa, Japan, 2019, pp. 082-085.
- [35] J. Li, X. Rao, S. Xiao, B. Zhao and D. Liu, "Pruner to Predictor: An Efficient Pruning Method for Neural Networks Compression," *2022 14th International Conference on Advanced Computational Intelligence (ICACI)*, Wuhan, China, 2022, pp. 9-14.
- [36] W. Luo, "Improving Neural Network With Uniform Sparse Connectivity," in *IEEE Access*, vol. 8, pp. 215705-215715, 2020.
- [37] Omar N., M. A. Monem, Y. Firouz, J. Salminen, J. Smekens, O. Hegazy, H. Gualous, G. Mulder, P. Van den Bossche, T. Coosemans, and J. Van Mierlo. "Lithium iron phosphate based battery — Assessment of the aging parameters and development of cycle life model." *Applied Energy*, Vol. 113, January 2014, pp. 1575–1585.
- [38] K. Wu, Y. Guo and C. Zhang, "Compressing Deep Neural Networks With Sparse Matrix Factorization," in *IEEE Transactions on Neural Networks and Learning Systems*, vol. 31, no. 10, pp. 3828-3838, Oct. 2020.
- [39] "Dataport Resources," May, 2019 [online] Available: <https://dataport.pecanstreet.org/academic>.
- [40] "ERCOT, Electric Reliability Council of Texas," [Online]. Available: <http://www.ercot.com/>.
- [41] "Pyomo, Python Software packages.," Available: [Online]. Available: <http://www.pyomo.org/>.
- [42] "Gurobi Optimization, Linear Programming Solver," [Online]. Available: <https://www.gurobi.com/>.
- [43] X. Li, A. Korad, and P. Balasubramanian, "Sensitivity Factors based Transmission Network Topology Control for Violation Relief," *IET Generation, Transmission & Distribution*, vol. 14, no. 17, pp. 3539-3547, Sep. 2020.